J|A|C|S
ARTICLES
Published on Web 04/21/2005

Design, Synthesis, Structure, and Gas (N_2, Ar, CO_2, CH_4, and H_2) Sorption Properties of Porous Metal-Organic Tetrahedral and Heterocuboidal Polyhedra

Andrea C. Sudik,[†] Andrew R. Millward,[†] Nathan W. Ockwig,[†] Adrien P. Côté,[†] Jaheon Kim,[‡] and Omar M. Yaghi*,[†]

Contribution from Materials Design and Discovery Group, Department of Chemistry, University of Michigan, Ann Arbor, Michigan 48109-1055, and Department of Chemistry, Soongsil University, Seoul 157-743, Korea

Received November 30, 2004; E-mail: oyaghi@umich.edu

Abstract: A strategy based on assembling metal ions and organic carboxylate links has been applied for the design and synthesis of a new class of porous, truncated tetrahedral and heterocuboidal polyhedra, whose pore size and functionality can be systematically varied. The synthesis of this series of metal-organic polyhedra (MOPs) employs sulfate-capped oxygen-centered iron-carboxylate trimers, $Fe_3O(CO_2)_3(SO_4)_3$, as rigid nodes separated by linear (phenyl, biphenyl, terphenyl, and tetrahydropyrene) or trigonal (benzenetriphenyl) links to yield five highly crystalline polyhedra of general formula $[NH_2(CH_3)_2]_8[Fe_{12}O_4(SO_4)_{12}(link)_x(py)_{12}]\cdot G$ ($x = 6$ for linear or 4 for trigonal, py = pyridine, G = guests). In this series, the size of each polyhedron has been varied from 20.0 to 28.5 Å (on edge), and the corresponding pore diameter from 7.3 to 13.3 Å. Gas sorption isotherms were measured for three members of this series to reveal significant uptake of gases (N_2, Ar, CO_2, H_2, CH_4) and benzene and exhibit Type I sorption behavior that is indicative of permanent porosity. The apparent surface areas for these compounds range from 387 to 480 m^2/g.

Extensive research has been devoted to the synthesis and characterization of metal-organic polygons and polyhedra (MOPs) such as squares, cubes, tetrahedra, and hexahedra.[1] Their structures have been constructed from nodes of either single metal ions or metal carboxylate clusters[2] that are joined by organic links. MOPs have voids within their structures where guest solvent molecules or counterions reside. Although reports of studies exploring the mobility of such guests have appeared,[3] the question of whether MOPs can support permanent porosity in the absence of guests remains unanswered. We believe that the utility of MOPs in catalysis, gas sorption, separation, and sensing applications hinges upon their ability to remain open in the absence of guests. In other words, their molecular structure should be architecturally robust to allow for removal of guests without destruction of the pores, precluding their use as porous polyhedra. Furthermore, MOPs with permanent porosity should allow for unhindered inclusion and removal of gas molecules as well as full access to adsorption sites within the pores.

In our work on metal-organic frameworks (MOFs), we have shown that employing metal carboxylate clusters instead of single metal ions as nodes yields stable architectures.[4] Here, we extend this strategy to MOPs in which the common oxygen-centered trinuclear clusters, $Fe_3O(CO_2)_6$, are employed as nodes (Figure 1a). The carboxylate carbon atoms are the points-of-extension that represent the vertexes of a trigonal prismatic secondary building unit (SBU) (Figure 1b). This SBU can be connected by polytopic links to give 3-D extended MOFs.[5] For example, this SBU can be joined by tritopic links at all six points-of-extension to yield an extended framework having a tetrahedral pore structure.[5c] In this study, three cofacial sites on the SBU have been capped by bridging sulfate groups to yield a triangular SBU (Figure 1c) which predisposes the

[†] University of Michigan.
[‡] Soongsil University.

(1) Squares: Fan, J.; Whiteford, J. A.; Olenyuk, B.; Levin, M. D.; Stang, P. J.; Fleischer, E. B. *J. Am. Chem. Soc.* **1999**, *121*, 2741. (b) Cubes: Sokol, J. J.; Shores, M. P. Long, J. R. *Inorg. Chem.* **2002**, *41*, 3052. Klausmeyer, K. K.; Rauchfuss, T. B.; Wilson, S. R. *Angew. Chem., Int. Ed.* **1998**, *37*, 1694. (c) Tetrahedra: Caulder, D.; Raymond, K. N. *Acc. Chem. Res.* **1999**, *32*, 975. (d) Hexahedra: Takeda, N.; Umemoto, K.; Yamaguchi, K.; Fujita, M. *Nature* **1999**, *398*, 794.

(2) Cotton, F. A.; Daniels, L. M.; Lin, C.; Murillo, C. A. *Chem. Commun.* **1999**, 841. (b) Cotton, F. A.; Lin, C.; Murillo, C. A. *Inorg. Chem.* **2001**, *40*, 6413. (c) Moulton, B.; Lu, J.; Mondal, A.; Zaworotko, M. J. *Chem. Commun.* **2001**, *9*, 863. (d) Eddaoudi, M.; Kim, J.; Wachter, J. B.; Chae, H. K.; O'Keeffe, M.; Yaghi, O. M. *J. Am. Chem. Soc.* **2001**, *123*, 4368. (e) Bourgeois, J. P.; Fujita, M.; Kawano, M.; Sakamoto, S.; Yamaguchi, K. *J. Am. Chem. Soc.* **2003**, *125*, 9260.

(3) Dinolfo, P. H.; Hupp, J. T. *Chem. Rev.* **2001**, *12*, 3113. (b) Keefe, M. H.; Slone, R. V.; Hupp, J. T.; Czaplewski, K. F.; Snurr, R. Q.; Stern, C. L. *Langmuir* **2000**, *16*, 3964. (c) Chatterjee, B.; Noveron, J. C.; Resendiz, M. J.; Liu, J.; Yamamoto, T.; Parker, D.; Cinke, M.; Nguyen, C. V.; Arif, A. M.; Stang, P. J. *J. Am. Chem. Soc.* **2004**, *126*, 10645.

(4) Li, H.; Eddaoudi, M.; Groy, T. L.; Yaghi, O. M. *J. Am. Chem. Soc.* **1998**, *120*, 8571. (b) Eddaoudi, M.; Li, H.; Yaghi, O. M. *J. Am. Chem. Soc.* **2000**, *122*, 1391. (c) Yaghi, O. M.; O'Keeffe, M.; Ockwig, N. W.; Chae, H. K.; Eddaoudi, M.; Kim, J. *Nature* **2003**, *423*, 705. (d) Eddaoudi, M.; Kim, J.; Rosi, N.; Vodak, D.; Wachter, J.; O'Keeffe, M.; Yaghi, O. M. *Science* **2002**, *295*, 469.

(5) Yang, G.; Raptis, R. G. *Chem. Commun.* **2004**, 2058. (b) Serre, C.; Millange, F.; Surblé, S.; Férey, G. *Angew. Chem., Int. Ed.* **2004**, *43*, 6285. (c) Férey, G.; Serre, C.; Mellot-Draznieks, C.; Millange, F.; Surblé, S.; Dutour, J.; Margiolaki, I. *Angew. Chem., Int. Ed.* **2004**, *43*, 6296. (d) Sudik, A. C.; Côté, A. P.; Yaghi, O. M. *Inorg. Chem.* **2005**, in press.

10.1021/ja042802q CCC: $30.25

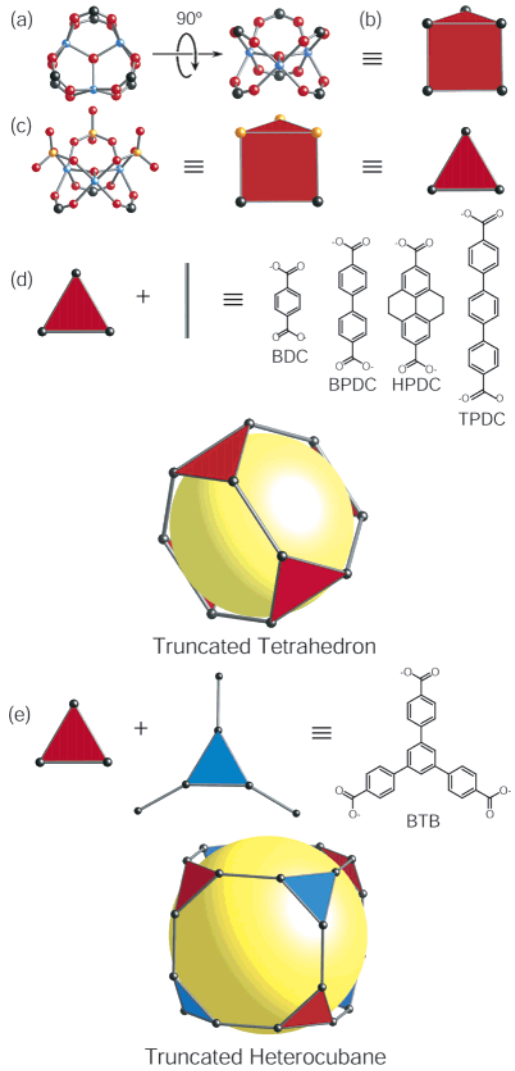

Figure 1. Schematic representation of the secondary building unit (SBU) approach used to prepare metal-organic polyhedra (MOPs). This strategy employs (a) $Fe_3O(CO_2)_6$ clusters (Fe, blue; O, red; C, black), (b) trigonal prismatic SBUs (red), that are (c) capped with sulfate (S, orange), yielding triangular SBUs (red). Linking these SBUs with either (d) linear (BDC, BPDC, HPDC, and TPDC) or (e) triangular (BTB) (blue) links produces truncated tetrahedral or heterocuboidal polyhedra, respectively. The yellow sphere within each polyhedron represents the size of the largest sphere that would occupy the cavity without contacting the interior van der Waals surface.

carboxylates at 60° to each other. Thus, linking these shapes together by either ditopic links such as 1,4-benzenedicarboxylate (BDC), 4,4′-biphenyldicarboxylate (BPDC), tetrahydropyrene-2,7-dicarboxylate (HPDC), and 4,4″-terphenyldicarboxylate (TPDC) or a tritopic link such as 1,3,5-tris(4-carboxyphenyl)-benzene (BTB) gives porous anionic truncated tetrahedra or a truncated heterocubane, respectively (Figure 1d,e).

We show that in this series of compounds the size of the pore and its opening can be systematically varied without altering the polyhedral shape. Specifically, the synthesis and single-crystal X-ray structures of each member of this series are described and, for three members, the gas sorption isotherms are reported. The latter data provide conclusive evidence that these discrete structures are architecturally robust and are indeed capable of gas adsorption typical of materials with permanent porosity.

Experimental Section

Methods, Materials, and Characterization of Compounds. Iron(III) sulfate hydrate, 1,4-benzenedicarboxylic acid (H_2BDC), 4,4′-biphenyldicarboxylic acid (H_2BPDC), and triethylamine (TEA) were purchased from Aldrich Chemical Co. and used as received without further purification. *N*,*N*-Dimethylformamide (DMF) (99.9%) and pyridine (py) (99.9%) were purchased from Fisher Chemicals. The organic acids, tetrahydropyrene-2,7-dicarboxylic acid (H_2HPDC),[6] 4,4″-terphenyldicarboxylic acid (H_2TPDC),[7] and 1,3,5-tris(4-carboxyphenyl)-benzene (H_3BTB),[8] were prepared according to published procedures. Elemental microanalyses of all products were performed at the University of Michigan, Department of Chemistry. Fourier transform infrared (FT-IR) spectra (4000−400 cm^{-1}) were obtained from KBr pellets using a Nicolet FT-IR Impact 400 system. Absorption peaks are described as follows: very strong (vs), strong (s), medium (m), and weak (w). Powder X-ray diffraction (PXRD) data were recorded on a Bruker AXS D8 Advance diffractometer operated at 1600 W power (40 kV, 40 mA) for Cu Kα (λ = 1.5406 Å), with a scan speed of 3°/min and a step size of 0.050° in 2θ. Simulated PXRD patterns were calculated using Powder Cell 2.2 from corresponding single-crystal structural models. Note that the crystallinity of all compounds is lost upon moderate or complete guest removal as well as mechanical sample grinding. Therefore, all PXRD experiments were performed on uncrushed, solvated samples. Although there are discrepancies between simulated and experimental PXRD patterns (due to differences in guest quantity/identity, low crystallinity, or preferred orientation), the reproducibility and correlation of observed lines with the simulated patterns can still aid in confirming bulk sample identity and purity (see Supporting Information for indexed PXRD patterns). Despite their noncrystallinity after evacuation of guests, MOP porosity is maintained, as evidenced by the reversible Type I behavior observed for uptake of gases (see Results and Discussion section).

Synthesis of Compounds. The synthetic methods used to obtain pure crystalline compounds and their characterization are described below. The addition of base (TEA) and stirring of metal salt and carboxylic acid link (24 to 72 h at room temperature) facilitate link deprotonation and homogeneous dispersion of reagents. All reactions and purification steps were performed under aerobic conditions unless otherwise noted. All compounds are insoluble in common polar and nonpolar organic solvents. Compounds are named as IRMOP-*n* or MOP-*n*, where IRMOP refers to isoreticular (having the same topology)[4d] metal-organic polyhedron and *n* is an integer assigned in roughly chronological order of discovery. We use the IRMOP designation for the truncated tetrahedral series, and MOP for the truncated heterocubane.

$[NH_2(CH_3)_2]_8[Fe_{12}O_4(BDC)_6(SO_4)_{12}(py)_{12}]\cdot G$, IRMOP-50. $Fe_2(SO_4)_3\cdot xH_2O$ (0.20 g, 0.50 mmol) and 1,4-benzenedicarboxylic acid (H_2BDC) (0.083 g, 0.50 mmol) were placed in a 50 mL round-bottom flask. DMF (50 mL) and TEA (130 μL) were added to the reaction flask. The heterogeneous reaction mixture was capped and allowed to stir for 24 h. A 6 mL aliquot of this mixture was placed in a glass scintillation vial (20 mL capacity) to which pyridine (4 mL) was added, capped, heated to 100 °C for 48 h, and removed to cool to room temperature. After 20 days, a few orange octahedral crystals of IRMOP-50 formed. Unlike other (IR)MOPs reported below, IRMOP-50 was difficult to obtain as a bulk material. Only enough material was isolated to complete single-crystal X-ray diffraction and FT-IR analysis. FT-IR (KBr 4000−400 cm^{-1}): 3436 (m), 3068 (m), 2939 (m), 2815 (w), 1658 (s), 1582 (vs), 1505 (m), 1436 (s), 1407 (vs), 1222 (s), 1147 (vs), 1035 (s), 993 (s), 830 (w), 750 (m), 685 (m), 663 (m), 597 (m), 555 (s), 479 (w).

(6) Connor, D. M.; Allen, S. D.; Collard, D. M.; Liotta, C. L.; Schiraldi, D. A. *J. Org. Chem.* **1999**, *64*, 6888. (b) Musa, A.; Sridharan, B.; Lee, H.; Mattern, D. L. *J. Org. Chem.* **1996**, *61*, 5481.
(7) Campbell, T. W. *J. Am. Chem. Soc.* **1960**, *82*, 3126.
(8) Elmorsy, S. S.; Pelter, A.; Smith, K. *Tetrahedron Lett.* **1991**, *32*, 4175.

$[NH_2(CH_3)_2]_8[Fe_{12}O_4(SO_4)_{12}(BPDC)_6(py)_{12}]\cdot G$, IRMOP-51 Triclinic and Cubic Forms. $Fe_2(SO_4)_3\cdot xH_2O$ (0.20 g, 0.50 mmol) and 4,4′-biphenyldicarboxylic acid (H_2BPDC) (0.12 g, 0.50 mmol) were placed in a 50 mL round-bottom flask. DMF (50 mL) and TEA (130 μL) were added to the reaction flask. The heterogeneous mixture was capped and allowed to stir for 24 h at room temperature. For the cubic phase, a 2.4 mL aliquot of the mixture was placed in a glass scintillation vial (20 mL capacity) to which pyridine (3.6 mL) was added. The vial was capped and heated to 100 °C for 48 h, then cooled to room temperature to give an orange crystalline solid of cubic IRMOP-51 (28% yield based on H_2BPDC). For the triclinic phase, a 1.5 mL aliquot of the heterogeneous mixture was placed in a Pyrex tube (i.d. × o.d. = 8 × 10 mm^2, 140 mm length) to which pyridine (1.5 mL) was added. The tube was subsequently flash frozen, evacuated, flame sealed, and heated to 115 °C (5 °C/min) for 40 h and cooled (0.5 °C/min) to room temperature. The resulting orange crystalline product was collected, washed with DMF (2 × 5 mL) and cyclohexane (2 × 5 mL) to give triclinic IRMOP-51 (38% yield based on H_2BPDC). High yields of crystalline IRMOP-51 phases are dependent upon heating under aerobic (cubic) or anaerobic (triclinic) conditions. All analytical characterization of this material was performed using the triclinic phase of IRMOP-51. Anal. Calcd for $C_{215}H_{347}N_{37}O_{121}Fe_{12}S_{12} = [NH_2(CH_3)_2]_8[Fe_{12}O_4(BPDC)_6(SO_4)_{12}(py)_{12}]\cdot(DMF)_{15}(py)_2(H_2O)_{30}$: C, 40.09; H, 5.43; N, 8.05. Found: C, 39.86; H, 5.48; N, 8.22. FT-IR (KBr, 4000−400 cm^{-1}): 3439 (s), 3068 (m), 2979 (m), 2941 (m), 2805 (m), 2737 (m), 2678 (m), 2491 (w), 1712 (w), 1655 (s), 1604 (s), 1592 (s), 1543 (m), 1494 (m), 1447 (m), 1418 (vs), 1226 (s), 1181 (m), 1143 (s), 1126 (vs), 1050 (s), 1037 (s), 983 (s), 860 (w), 845 (w), 795 (w), 774 (m), 702 (m), 681 (m), 661 (m), 601 (s), 476 (m).

$[NH_2(CH_3)_2]_8[Fe_{12}O_4(SO_4)_{12}(HPDC)_6(py)_{12}]\cdot G$, IRMOP-52. Equimolar amounts of $Fe_2(SO_4)_3\cdot x(H_2O)$ (0.05 g, 0.13 mmol) and tetrahydropyrene-2,7-dicarboxylic acid (H_2HPDC) (0.04 g, 0.13 mmol) were suspended at room temperature in a 50 mL round-bottom flask containing DMF (20 mL) and pyridine (20 mL). TEA (50 μL) was added to this mixture. The reaction flask was capped and stirred at room temperature for 72 h. A 1.2 mL aliquot of the stirring heterogeneous reaction mixture was placed in a Pyrex tube (i.d. × o.d. = 8 × 10 mm^2, 140 mm length) followed by addition of pyridine (1.8 mL). The tube was subsequently flash frozen, evacuated, flame sealed, and heated to 115 °C (5 °C/min) for 32 h. Upon cooling to room temperature (0.5 °C/min) and allowing the reaction to stand for several weeks, an orange crystalline solid of IRMOP-52 formed from the orange solution. Crystalline IRMOP-52 product was purified by density separation (bromoform/CH_2Cl_2). The isolated product (5% based on H_2HPDC) was washed with DMF (3 × 5 mL) and cyclohexane (1 × 5 mL). Anal. Calcd for $C_{211}H_{319}O_{115}N_{29}S_{12}Fe_{12} = [NH_2(CH_3)_2]_8[Fe_{12}O_4(HPDC)_6(SO_4)_{12}(py)_{12}]\cdot(DMF)_9(H_2O)_{30}$: C, 41.16; H, 5.22; N, 6.60. Found: C, 41.15; H, 5.32; N, 6.86. FT-IR (KBr, 4000−400 cm^{-1}): 3433 (s), 3070 (m), 2937 (m), 2894 (m), 2834 (m), 1643 (m), 1605 (s), 1584 (s), 1544 (s), 1486 (m), 1466 (s), 1433 (s), 1404 (vs), 1352 (m), 1225 (s), 1127 (vs), 1066 (s), 1039 (vs), 984 (s), 791 (w), 752 (m), 701 (m), 604 (s), 476 (m).

$[NH_2(CH_3)_2]_8[Fe_{12}O_4(SO_4)_{12}(TPDC)_6(py)_{12}]\cdot G$, IRMOP-53. $Fe_2(SO_4)_3\cdot xH_2O$ (0.19 g, 0.47 mmol) and 4,4″-terphenyldicarboxylic acid (H_2TPDC) (0.15 g, 0.47 mmol) were placed in a 50 mL round-bottom flask, to which DMF (15 mL), pyridine (15 mL), and TEA (130 μL) were added. The heterogeneous reaction mixture was capped and allowed to stir at room temperature for 24 h. A 6 mL aliquot of the stirring mixture and pyridine (4 mL) were added to a glass scintillation vial (20 mL capacity). The vial was capped and heated to 105 °C (5 °C/min) for 24 h and cooled (0.5 °C/min) to room temperature to give an orange-red solution. After 4 days at room temperature, the orange product crystallized as plates of IRMOP-53 (31% yield based on H_2TPDC). Crystals of IRMOP-53 were isolated and washed with pyridine (3 × 10 mL) and cyclohexane (1 × 10 mL). Anal. Calcd for $C_{252}H_{274}N_{28}O_{77}Fe_{12}S_{12} = [NH_2(CH_3)_2]_8[Fe_{12}O_4(SO_4)_{12}(TPDC)_6(py)_{12}]\cdot(py)_7(DMF)(C_6H_{12})_3$: C, 50.60; H, 4.62; N, 6.56. Found: C, 50.59; H, 4.39; N, 6.48. FT-IR (KBr, 4000−400 cm^{-1}): 3427 (s), 3074 (m), 2983 (m), 2807 (m), 2499 (w), 1607 (vs), 1593 (vs), 1555 (s), 1422 (vs), 1226 (s), 1146 (vs), 1120 (vs), 1038 (s), 1009 (s), 985 (s), 844 (w), 786 (s), 708 (m), 603 (m), 547 (m).

$[NH_2(CH_3)_2]_8[Fe_{12}O_4(SO_4)_{12}(BTB)_4(py)_{12}]\cdot G$, MOP-54. A 3:2 molar ratio of $Fe_2(SO_4)_3\cdot x(H_2O)$ (0.06 g, 0.15 mmol) and 1,3,5-tris(4-carboxyphenyl)benzene (H_3BTB) (0.044 g, 0.10 mmol) was suspended in a 20 mL solution of a 1:1 DMF/pyridine solution using a 50 mL round-bottom flask. TEA (150 μL) was added, and the reaction capped and stirred at room temperature for 72 h. A 3 mL aliquot of the stirring heterogeneous mixture was placed in a Pyrex tube (i.d. × o.d. = 8 × 10 mm^2, 140 mm length). The tube was flash frozen, evacuated, flame sealed, and heated to 115 °C (5 °C/min) for 42 h and cooled (0.5 °C/min) to room temperature. Octahedral orange crystals of MOP-54, which formed during the isotherm, were purified by density separation (bromoform/pyridine). The isolated product (20% yield based on H_3BTB) was washed with pyridine (3 × 5 mL) and cyclohexane (1 × 5 mL). Anal. Calcd for $C_{230}H_{308}N_{34}O_{103}Fe_{12}S_{12} = [NH_2(CH_3)_2]_8[Fe_{12}O_4(BTB)_4(SO_4)_{12}(py)_{12}]\cdot(DMF)_{12}(py)_2(H_2O)_{15}$: C, 44.19; H, 4.97; N, 7.63. Found: C, 44.15; H, 5.06; N, 7.63. FT-IR (KBr, 4000−400 cm^{-1}): 3425 (vs), 2841 (s), 2809 (m), 2683 (m) 2490 (w), 1715 (m), 1661 (vs), 1611 (s), 1550 (m), 1535 (m), 1413 (vs), 1214 (s), 1125 (vs), 1067 (s), 1036 (s), 991 (s), 857 (m), 810 (m), 785 (s), 701 (m), 665 (m), 607 (s), 505 (s), 417 (m).

Single-Crystal X-ray Diffraction Studies. The crystallographic measurements were made on a Bruker SMART APEX CCD area detector with graphite-monochromated Mo Kα radiation ($\lambda = 0.71073$ Å) operated at 2000 W power (50 kV, 40 mA). Data collection was performed on specimens sealed in glass capillaries at 258(2) K unless otherwise noted. All structures were solved by direct methods and subsequent difference Fourier syntheses using the SHELX-TL software suite. Non-hydrogen atoms of the anionic polyhedral fragments and coordinated pyridines were refined anisotropically (unless disordered) with hydrogen atoms generated as spheres riding the coordinates of their parent atoms.

For all structures it was difficult to locate and resolve guest molecules, as more than 50% of the crystal was comprised of disordered solvent. This was responsible for the elevated residuals reported. In all cases (except cubic IRMOP-51) it was more reasonable to model data collected at elevated temperatures (≥−15 °C) when guest entities in the structures where allowed to move freely and therefore did not contribute coherent scattering terms to the observed structure factors. Conversely, at cryogenic temperatures free solvent in the crystals will "freeze" into nonordered arrays within the pore structure. In such cases the modeling of the disordered guest entities becomes intractable. Compounding the disorder problem is the scattering ability of the single crystalline forms, which were small and weakly diffracting (attempts to grow larger crystals generated samples with less crystallinity) and did not display quality high-angle data (>1 Å). The reason for this is twofold. First, as is inherent to small crystals, longer exposure times are required to increase the intensity of high-angle data; however, in these cases prolonged exposure times (> 60 s/frame) resulted in saturation of the CCD detector by strong low angle scattering. Second, the large degree of diffuse scattering from the disordered solvent produces a large background and masked high-angle data. When possible, information for each structure is given before and after being subjected to the SQUEEZE subroutine of PLATON (see Table 1).[9] Reduced residuals for the SQUEEZED structures further confirm that primary uncertainty in the crystallographic models stems from the disordered guests in the large void spaces and not the polyhedral fragment.

Magnetic Measurements. Magnetic measurements were performed using a Quantum Design MPMS-2S SQUID magnetometer. Approximately 10 mg of evacuated sample was packed under inert

(9) Spek, A. L. *J. Appl. Crystallogr.* **2003**, *36*, 7.

Table 1. Single Crystal X-ray Data for IRMOP-50 to -53 and MOP-54

	IRMOP-50	triclinic IRMOP-51	cubic IRMOP-51[a]	IRMOP-52	IRMOP-53	MOP-54
empirical formula[b]	$C_{108}H_{84}N_{12}O_{88}S_{12}Fe_{12}$	$C_{212.5}H_{100}N_{36.5}O_{90}S_{12}Fe_{12}$	$C_{150}H_{108}N_{18}O_{76}S_{12}Fe_{12}$	$C_{226}H_{132}N_{26}O_{94}S_{12}Fe_{12}$	$C_{188.5}H_{132}N_{13.5}O_{104.5}S_{12}Fe_{12}$	$C_{180}H_{120}N_{16}O_{115}S_{12}Fe_{12}$
fw[b]	4012.89	5659.21	4433.46	5770.50	5313.12	5401.84
cryst size, mm	$0.21 \times 0.18 \times 0.17$	$0.34 \times 0.25 \times 0.08$	$0.10 \times 0.10 \times 0.10$	$0.22 \times 0.15 \times 0.04$	$0.43 \times 0.22 \times 0.09$	$0.20 \times 0.20 \times 0.20$
cryst syst/s.g.	cubic, $F\bar{4}3m$	triclinic, $P\bar{1}$	cubic, $F\bar{4}3m$	monoclinic, $C2/c$	triclinic, $P\bar{1}$	tetragonal, $I4_1/a$
T, K	258(2)	293(2)	153(2)	258(2)	293(2)	258(2)
a, Å	32.650(1)	25.8626(9)	38.508(9)	43.730(4)	31.642(3)	26.854(1)
b, Å	32.650(1)	26.8359(9)	38.508(9)	22.671(2)	31.762(3)	26.854(1)
c, Å	32.650(1)	28.192(1)	38.508(9)	41.328(4)	31.830(3)	40.922(2)
α, deg	90	75.138(1)	90	90	75.847(2)	90
β, deg	90	88.568(1)	90	120.182(2)	75.264(2)	90
γ, deg	90	63.783(1)	90	90	60.155(2)	90
V, Å^3	34 807(2)	16 878(1)	57 100(2)	35 418(6)	26 568(4)	29 512(2)
Z	4	2	4	4	2	4
d_{calc}, g/cm^3	0.766	1.114	0.516	1.082	0.664	1.216
μ, mm^{-1}	0.605	0.645	0.370	0.616	0.408	0.738
reflns collected	59 634	106 447	29 975	85 593	216 921	85 438
unique reflns	3845	48 424	3927	29 981	94 138	17 618
restraints	4	102	4	6	0	2
params	100	2 632	122	1256	2217	728
R1, *w*R2(all), %[c]	9.79, 30.60 [4.59, 7.81]	10.32, 33.87 [5.50, 10.86]	8.65, 27.78 [7.70, 23.09]	14.71, 46.96 [7.36, 16.12]	12.61, 41.62 [5.85, 15.04]	8.34, 28.90[d]
GOF[c]	1.668 [0.939]	1.046 [0.940]	1.005 [0.838]	1.018 [0.853]	1.133 [0.710]	1.006[d]

[a] Twinned crystal. Note: application of SQUEEZE is not as effective for twinned data. [b] For non-SQUEEZED data. [c] Statistics following treatment of data with SQUEEZE subroutine of PLATON are bracketed. [d] The SQUEEZE subroutine of PLATON could not be applied because it could not fully model void space in this structure.

atmosphere into the sample holder and loaded into the magnetometer. A plot of magnetization versus field for data at 5, 10, 50, 150, and 250 K was found to be linear up to 15 kG. Therefore, variable-temperature magnetic susceptibility measurements were performed in the temperature range of 5−300 K at a constant magnetic field of 5 kG. A total of 64 data points were collected for each sample. All measurements were corrected for diamagnetic contribution from the sample holder while core diamagnetic contributions were calculated using Pascal's constants to obtain the molar susceptibilities (χ_m).

Gas Sorption Isotherms (0 to 1 bar). A sample of MOP in chloroform was transferred by a pipet to a quartz bucket and suspended in a previously described sorption apparatus.[4b] Excess solvent was removed from the crystals at ambient temperature and 10^{-3} Torr until no further weight loss occurred. Liquid nitrogen was used for N_2 and Ar sorption isotherms (−195 °C), while an acetone/dry ice slush was used for the CO_2 isotherm (−78 °C). The N_2 and Ar gases used were UHP grade, while the CO_2 was of 99.8% purity. Benzene was purchased as anhydrous GC grade (99.8%) from Aldrich Chemical Co.

The adsorbate was dosed to the sample while monitoring mass, pressure, and temperature. An isothermal data point (P_{eq},W_{eq}) was logged when the mass change was <0.01 mg/300 s. All data points were corrected for buoyancy and plotted versus relative pressure (P/P_o). Buoyancy corrections were determined from the slope (m_{buoy}) of the isotherm obtained by a standard aluminum foil weight and applied to equilibrium pressure-weight data points as $W_{buoy} = W_{eq} - m_{bouy} \times P_{eq}$. The BET surface area ($A_s$) was calculated from N_2 isotherm points within the range of 0.005−0.032 P/P_o, assuming an N_2 cross-sectional area of 16.2 Å^2/molecule. The pore volume (V_p) was determined by extrapolating the Dubinin−Radushkevich equation across the linear region of the low-pressure data points with the assumption that the density of the adsorbate in the pore was the same as that of the pure adsorbate in its liquid state.[10] For all calculations reported on a per volume basis, it was assumed that all free, neutral guests were removed and the unit cell volumes were maintained during evacuation.

For the hydrogen adsorption isotherms, the gas manifold was modified with a U-tube filled with molecular sieves. The sieves were flame-heated under vacuum, then immersed in a liquid nitrogen bath. Prepurified H_2 was passed through the sieves before entering the sample chamber.

Gas Sorption Isotherms (0 to 35 bar). A 50−70 mg evacuated sample was charged with ca. 40 Torr benzene while still in the low-pressure sorption apparatus mentioned above. Then the sample chamber was brought to ambient pressure with nitrogen. The benzene-filled sample was quickly transferred to a hemispherical quartz bucket (10 mm diameter, approximately 30 mg). The loaded bucket was suspended from a fused quartz spring and enclosed in a Ruska Mass-Sorption System (model 4403−800) outfitted with a Druck DPI 260 pressure gauge and PDCR 4010 pressure transducer. The sample was evacuated overnight until the cathetometer (0.02 mm sensitivity) showed no further change in bucket height, whereupon the initial height (weight) was recorded. Doses of UHP methane were sequentially introduced to the sample at room temperature while monitoring the system pressure, temperature, and sample height. Equilibrium was assumed when cathometer readings at 5-min intervals showed no detectable change. Heights were converted to weights based on the spring constant ($k \approx$ 0.500 mg/mm, calibrated per sample with standard aluminum foil weights); all data points were corrected for buoyancy as above and plotted versus increasing pressure.

Results and Discussion

Many studies have shown how organic carboxylate links can be used to provide the required angles between paddle-wheel clusters (square SBUs) in the assembly of both metal-organic

(10) Rouquerol, F.; Rouquerol, J.; Sing, K. *Adsorption by Powders & Porous Solids*; Academic Press: London, UK, 1999.

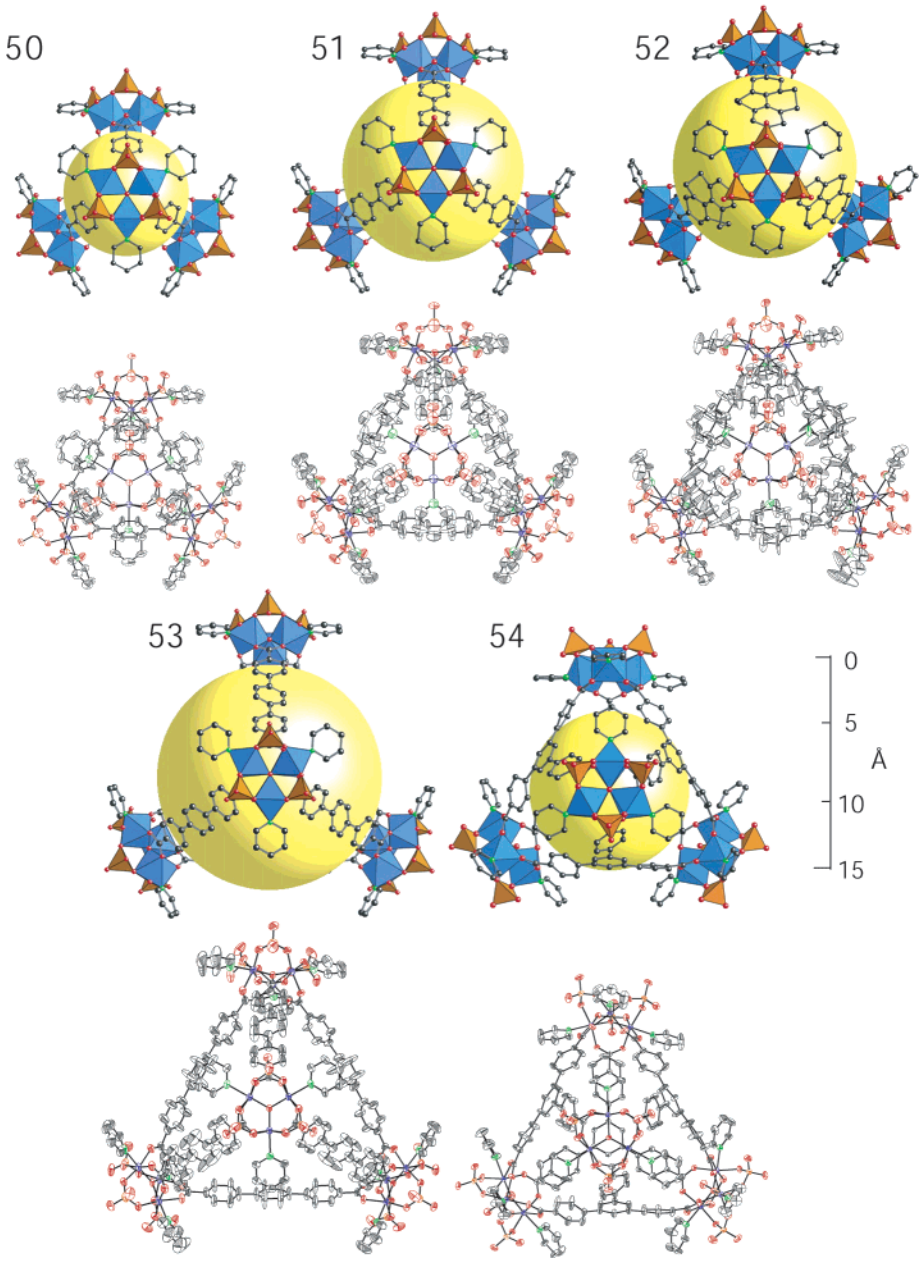

Figure 2. Single-crystal X-ray structures accompanied by ORTEP representations (at 30% probability level) of IRMOP-50 to -53 and MOP-54 (Fe, blue polyhedra; S, orange polyhedra; O, red spheres; N, green spheres; C, gray spheres). The large yellow spheres are as in Figure 1. All hydrogen atoms and guests have been omitted, and only one orientation of the disordered link atoms in IRMOP-52 is shown for clarity. Only the structure of cubic phase of IRMOP-51 is shown here.

polyhedra (MOPs) and extended metal-organic frameworks (MOFs).[2a−d,11] This study presents the utility of carboxyl groups of the capped triangular $Fe_3O(CO_2)_3(SO_4)_3$ unit (Figure 1) in providing the necessary 60° angles which are ideally suited for building truncated tetrahedral and heterocuboidal shapes with linear or trigonal organic links.

At the outset, a large number of exploratory reactions were carried out in order to identify the conditions that yield the sulfate-capped trigonal $Fe_3O(CO_2)_3(SO_4)_3$ unit in the presence of an organic carboxylate. This was successfully achieved by reacting $Fe_2(SO_4)_3 \cdot xH_2O$ and 4,4′-biphenyldicarboxylic acid in a solution of pyridine, *N*,*N*-dimethylformamide, and triethylamine at 100−115 °C. These conditions, which yield IRMOP-51, were subsequently used (with slight modification and substitution of the desired link) in the synthesis of the entire metal-organic polyhedral series (IRMOP-50 to 53 and MOP-54).

Synthesis and Composition of Compounds. With the exception of IRMOP-50, all polyhedra were prepared as bulk crystalline materials. Their single-crystal X-ray structures and details of the experiments are shown in Figure 2 and Table 1, respectively. The vertexes of each member of this series are composed of $Fe_3O(CO_2)_3(SO_4)_3(py)_3$ units with the bridging sulfates acting as capping groups that prevent the formation of extended structures. Thus the $Fe_3O(CO_2)_3$ is a triangular SBU that is connected to three ditopic (IRMOP-50 to 53) or tritopic (MOP-54) organic links. In all cases the coordination sphere of each metal is completed by a terminal pyridine ligand to

(11) Eddaoudi, M.; Kim, J.; Vodak, D.; Sudik, A.; Wachter, J.; O'Keeffe, M.; Yaghi, O. M. *Proc. Natl. Acad. Sci. U.S.A.* **2002**, *99*, 4901.

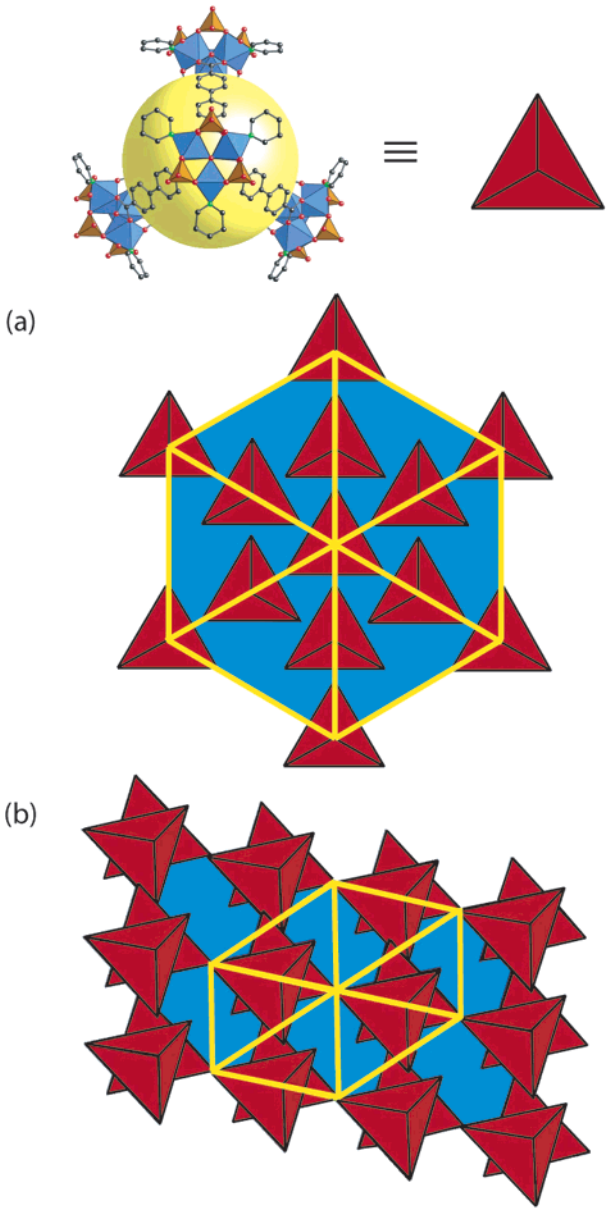

Figure 3. Representation of (a) the face-centered cubic (along 3-fold body diagonal) and (b) the triclinic crystal packing arrangements of tetrahedra as observed in the cubic and triclinic forms of IRMOP-51. The relative contributions of pore A (red) and pore B (blue) are illustrated with respect to the unit cell volume (outlined in yellow). The vertexes of the red tetrahedra are drawn using the crystallographic positions of the central oxygen atoms of the $Fe_3O(CO_2)_3(SO_4)_3$ clusters.

give an overall octahedral Fe center. The anionic charge (−8 per polyhedron) is balanced by dimethylammonium guests whose formation is based on the well-established decarbonylation of DMF upon heating in the presence of base.[12] Comparison of pK_b values of pyridine (8.81) and dimethylamine (3.27) guests is consistent with the dimethylammonium counterion assignment.[13] In general, it is difficult to completely formulate the composition of all the guests in such polyhedra due to the volatility of the guest molecules, an aspect that is commonly encountered in the analogous MOF chemistry. In addition, disorder in the single-crystal X-ray diffraction data often prevents definitive assignment of guest molecules (see Experimental Section for details). Elemental microanalysis has limited utility in this context since the guests contain some of the elements that are also present in the polyhedra. Nevertheless, given that the guests will ultimately be evacuated or exchanged from the pores, and that the structures of the polyhedra have been determined definitively from the single-crystal X-ray diffraction data, any ambiguity in the formulation of guest molecules does not preclude the use of such polyhedra as porous materials.

Table 2. Metrics of Metal-Organic Polyhedra

	IRMOP-*n*, MOP-*n*					
	50	51 (cubic)	51 (triclinic)	52	53	54
van der Waals length of edge (Å)	20.0	24.2	24.2	24.1	28.5	24.3
free diameter pore A (Å)[a]	3.8	6.4	6.4	4.0	9.4	3.6
fixed diameter pore A (Å)[b]	7.3	10.4	10.3	10.4	13.3	9.3
% free volume pore A[c]	7.1	13.7	23.1	19.4	26.7	19.1
% free volume pore B[c]	58.9	62.7	34.6	37.7	43.8	27.2
% free volume total (pore A + pore B)[c]	66.3	76.4	57.7	57.1	70.5	46.3

[a] Cerius2 measurements calculated by diameter of sphere that can pass through the aperture of pore A without contacting the van der Waals surface of the polyhedron (including axial py molecules). [b] Measurements calculated with PLATON using "cavity plt" function. [c] % free volume calculations performed with PLATON using "calc solv" function with a 1.4 Å probe radius and replacing organic cations in pore B with H^+.

Magnetic Measurements. To determine whether the magnetic behavior of the Fe carboxylates in these polyhedra is consistent with that of the unlinked molecular counterparts, we measured their magnetic susceptibilities. For IRMOP-51, IRMOP-53, and MOP-54 the studies were performed in the temperature range of 5−300 K at a constant magnetic field of 5 kG. At 300 K the effective magnetic moments (μ_{eff}) per iron center for IRMOP-51 (3.80 μ_B), IRMOP-53 (3.33 μ_B), and MOP-54 (3.29 μ_B) are considerably smaller than the calculated spin-only value (5.92 μ_B) for three uncoupled $S = 5/2$ iron centers, but fall within the range expected for molecular $[Fe^{III}_3O(RCO_2)_6L_3]^+$ systems (3.0 to 3.9 μ_B).[14] All compounds exhibit a gradual decrease in magnetic moment to 1.85 μ_B (IRMOP-51), 1.44 μ_B (IRMOP-53), and 1.46 μ_B (MOP-54) at 5 K, indicating antiferromagnetic interactions between iron centers. The low-temperature μ_{eff} values do not extrapolate toward zero and are consistent with previously reported molecular species. On the basis of this correlation between experimental and literature data and as similarly observed in analogous discrete polyhedral or infinite assemblies, long-range coupling between clusters is presumed to be negligible.[15]

Molecular Structure, Crystal Packing, and Variation of Metrics. The packing of the polyhedra in their crystalline forms reveals two kinds of pores within each crystal structure as illustrated for the cubic and triclinic phases of IRMOP-51 (Figure 3a,b, respectively). The first, pore A, is located within the truncated polyhedra, while the second, pore B, is the space between the polyhedra. The relative space provided by pore A

(12) Wan, Y.; Alterman, M.; Larhed, M.; Hallberg, A. *J. Org. Chem.* **2002**, *67*, 6232. (b) Perrin, D. D.; Armarego, W. L. F. *Purification of Laboratory Chemicals*, 3rd ed.; Pergamon: Oxford, 1988.
(13) *CRC Handbook of Chemistry and Physics*, 72nd ed.; Lide, D. R., Ed.; CRC Press: 1991−1992.
(14) Cannon, R. D.; White, R. P. *Prog. Inorg. Chem.* **1988**, *36*, 195.
(15) Barthelet, K.; Riou, R.; Férey, G. *Chem. Commun.* **2002**, 1492. (b) Saalfrank, R. W.; Glaser, H.; Demleitner, B.; Hampel, F.; Chowdhry, M. M.; Schünemann, V.; Trautwein, A. X.; Vaughan, G. B. M.; Yeh, R.; Davis, A. V.; Raymond, K. N. *Chem. Eur. J.* **2002**, *8*, 493.

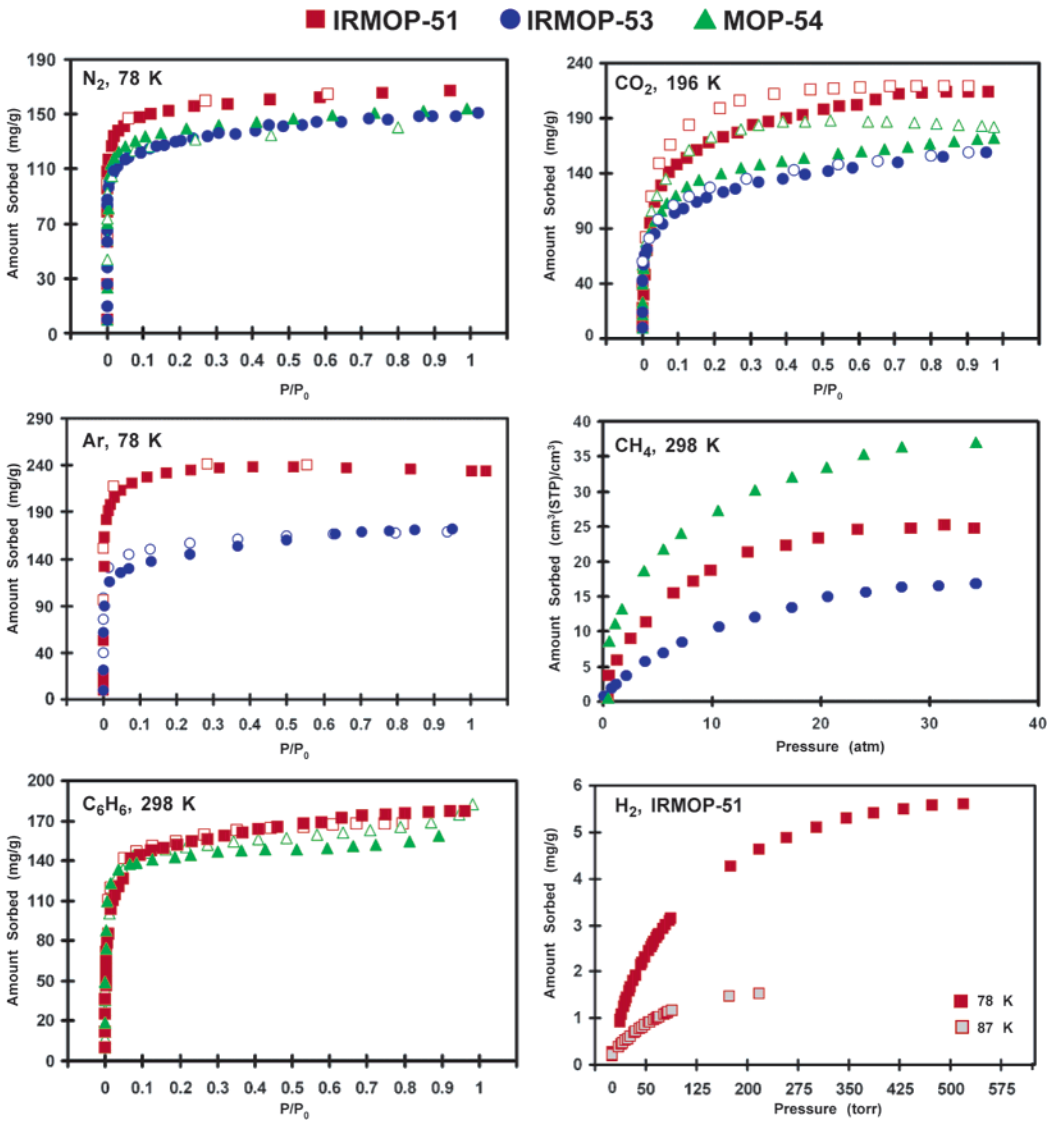

Figure 4. Gas and organic vapor sorption isotherms (filled points, sorption; open points, desorption) for IRMOP-51 (red squares), IRMOP-53 (blue circles), and MOP-54 (green triangles). P/P_o is the ratio of gas pressure (P) to saturation pressure (P_o).

and pore B in the polyhedral series is ultimately dependent upon their packing arrangement. The most densely packed arrangement exists for MOP-54 in which the truncated heterocubanes fall on the nodes of a diamond net (**dia**). The cubic phases of IRMOP-50 and -51 are exceptionally less dense. Here, tetrahedra are widely spaced, and the centers of the tetrahedra are located at the nodes of a face-centered cubic net (Figure 3a). The vertexes of the tetrahedra (taken as the three-coordinated O at the center of the Fe carboxylate cluster) form a cristobalite net (**crs**).[16] For all polyhedra, the two types of pores are interconnected by virtue of each truncated polyhedron having four open triangular faces (IRMOP-50 to IRMOP-53) or six open edges (MOP-54).

As expected from this series, linker length and width have a pronounced impact on the pore metrics, as summarized in Table 2. We note that the size of the polyhedra on an edge ranges from 20.0 to 28.5 Å, and the free pore diameter of pore A ranges from 3.6 to 9.4 Å, while the fixed pore diameter of pore A ranges from 7.3 to 13.3 Å. The volume of space within the polyhedra (pore A) is modulated from 7.1 to 26.7% of the total crystal volume. However, the volume of space between the polyhedra (pore B) is significantly larger than that found within the polyhedra (pore A), as it ranges from 27.2 to 62.7% of the total crystal volume. While the dimethylammonium counterions represent <6% of the total volume when included in the calculations, their location has a significant impact on the volume that can be *accessed* by incoming guest molecules by potentially obstructing access to pore A or B. The total open space (pore A + pore B) in the crystals of this series represents a significant portion of crystal volume, ranging from 46.3 to 76.4%.

Establishing Permanent Porosity of Metal-Organic Polyhedra. To determine whether these structures have architectural rigidity and permanent porosity, we measured the gas adsorption isotherms of evacuated samples of IRMOP-51 (triclinic), -53, and MOP-54 (Figure 4, Table 3). The N_2 sorption at 78 K for all three compounds revealed reversible Type I isotherms, which are characteristic of microporous materials. Respective N_2 uptakes of 101, 57, and 109 $cm^3(STP)/cm^3$ are observed that correspond to 23, 20, and 22 N_2 molecules per formula unit

(16) O'Keeffe, M.; Hyde, B. G. *Crystal Structures: I. Patterns and Symmetry*; Mineralogical Society of America: Washington, DC, 1996.

Table 3. Sorption Data for Metal-Organic Polyhedra

IRMOP-*n*, MOP-*n*	guest	uptake (cm^3 STP/cm^3)	guest/f.u.[a]	A_s (m^2/g)	V_p (cm^3/cm^3)
51	N_2	101	23	480	0.18
	Ar	106	24		0.16
	CO_2	74	17		0.16[b]
	C_6H_6	0.14	8		0.17
	CH_4	25 (35 atm)	5.6		
	H_2[c]	54.9	12.5		
53	N_2	57	20	387	0.10
	Ar	42	15		0.07
	CO_2	32	12		0.06[b]
	CH_4	17 (35 atm)	5.9		
54	N_2	109	22	424	0.20
	CO_2	63	13		0.14[b]
	C_6H_6	0.18	9		0.20
	CH_4	37 (35 atm)	7.3		

[a] f.u. = one truncated polyhedron (including counterions and ligated py) = $[(CH_3)_2NH_2]_8[Fe_{12}O_4(link)_x(py)_{12}(SO_4)_{12}]$ ($x = 6$ for IRMOP-51 and IRMOP-53; $x = 4$ for MOP-54). [b] Density of liquid CO_2 at triple point = 1.18 g/cm^3. [c] H_2 values reported at 500 Torr and 78 K.

(Table 3).[17] Using the BET model, the apparent surface areas (A_s) of IRMOP-51, -53, and MOP-54 were calculated to be 480, 387, and 424 m^2/g, respectively. By extrapolation of the Dubinin−Radushkevich (DR) equation, the respective pore volumes (V_p) were estimated to be 0.18, 0.10, and 0.20 cm^3/cm^3.

These compounds also show Type I isotherms upon exposure to Ar, CO_2, and C_6H_6 vapor (Figure 4). Gradual hysteresis and incomplete desorption are evident in the CO_2 isotherms, a behavior previously observed in MOFs.[18] Since CO_2 has a small kinetic diameter (3.3 Å), we speculate that such behavior is a result of the increased sorbate−sorbent interactions as the molecules access more acute pores. For all adsorbates, the sorption capacity of pore B sorption is difficult to assess. As discussed in the Experimental Section, the packing of polyhedra in the solid is random after desolvation, an indication of the weak forces between discrete units. Nevertheless since these materials are porous, their molecular porosity (pore A) is certainly maintained in the absence of neutral guests even though the size of pore B may change. Also, as the location of counterions may hinder gas diffusion and potentially occlude pore A or B sorptive sites, future studies will explore the influence of counterions and pore type on gas sorption properties.

In the area of microporous materials a wealth of conceptual approaches have been developed for preparing extended structures with high porosity and reversible Type I behavior. For zeolites, apparent surface areas up to 500 m^2/g (Faujasite) and pore volumes up to 0.47 cm^3/cm^3 (zeolite A) have been reported.[19] Metal-organic frameworks have been designed with apparent surface areas and pore volumes up to 4500 m^2/g and 0.69 cm^3/cm^3 (MOF-177).[20] While gas uptake in metal-organic polygonal and polyhedral assemblies has been investigated, to our knowledge reversible Type I behavior and thus permanent porosity has not been demonstrated. We speculate that such lack of permanent porosity is attributed to the flexible nature of single metal ion vertexes. In this study, the SBU approach has been successfully applied to generate a series of discrete, porous polyhedra with reversible Type I behavior as well as apparent surface areas comparable to MOFs and some of the most porous zeolites.

To examine the potential utility of this series in the storage of gas fuels, IRMOP-51, -53, and MOP-54 were subjected to high-pressure CH_4 sorption at room temperature. All materials were nearly saturated at 35 atm, with respective uptakes of 25, 17, and 37 cm^3(STP)/cm^3. These uptake values correspond to approximately 5.6 (IRMOP-51), 5.9 (IRMOP-53), and 7.3 (MOP-54) methane molecules per formula unit. Furthermore, the hydrogen uptake of IRMOP-51 was measured at 78 and 87 K: the maximum uptake at each of the two given temperatures is 54.9 and 13.5 cm^3(STP)/cm^3, equivalent to 12.5 and 3.1 H_2 molecules per formula unit. For comparison, MOF-5 takes up 67.4 cm^3(STP)/cm^3 at 78 K and 500 torr.[21] Thus, on a per volume basis, IRMOP-51 is comparable with MOF-5, having 81% of its hydrogen capacity in this temperature−pressure regime.

The isosteric heat of adsorption (q_{st}) reflects the enthalpy change during the initial surface coverage and is a measure of the strength of the sorbate−sorbent interaction. Employing the Clausius−Clapeyron equation in conjunction with the 78 and 87 K hydrogen isotherms for IRMOP-51, q_{st} was calculated to be 10.9 ± 1.9 kJ/mol. This value is higher than those for activated carbons (6.4 kJ/mol) and planar graphite (4 kJ/mol), yet lower than some reported values for SWNT (19.6 kJ/mol).[22] For more favorable uptake, the sorbate−sorbent interaction (q_{st}) could potentially be increased to enable a material to reach its uptake capacity more efficiently, while allowing desorption to occur under moderate conditions. The comparable hydrogen uptakes of IRMOP-51 and MOF-5 could be attributed to the relative high isosteric heat of IRMOP-51.

Summary

This study has demonstrated (a) application of the SBU approach to the design and synthesis of metal-organic truncated tetrahedral and truncated heterocuboidal polyhedra, (b) systematic control over their metrics, and (c) their rigid molecular structures and permanent porosity by measurement of their gas adsorption.

Acknowledgment. This work was supported by the National Science Foundation (DMR 0242630) and the Department of Energy (DOE). We thank Professor Michael O'Keeffe (Arizona State University) for his invaluable comments and Dr. Ulrich Müller (BASF, Ludwigshafen) for his assistance in corroborating the hydrogen measurements. A.P.C. thanks Science and Engineering Research Canada (NSERC) for a postdoctoral fellowship.

Supporting Information Available: Table summarizing synthetic conditions of all compounds. Details of single-crystal

(17) One formula unit (one polyhedron) is $[(CH_3)_2NH_2]_8[Fe_{12}O_4(link)_x(py)_{12}(SO_4)_{12}]$ ($x = 6$ for IRMOP-51 and IRMOP-53; $x = 4$ for IRMOP-54).
(18) Dybtsev, D. N.; Chun, H.; Yoon, S. H.; Kim, D.; Kim, K. *J. Am. Chem. Soc.* **2004**, *126*, 32.
(19) Breck, D. W. *Zeolite Molecular Sieves*; Wiley & Sons: New York, 1974.
(20) Chae, H. K.; Siberio-Pérez, D. Y.; Kim, J.; Go, Y.; Eddaoudi, M.; Matzger, A. J.; O'Keeffe, M.; Yaghi, O. M. *Nature* **2004**, *427*, 523.
(21) Rowsell, J. L. C.; Millward, A. R.; Park, K. S.; Yaghi, O. M. *J. Am. Chem. Soc.* **2004**, *126*, 5666.
(22) Bénard, P.; Chahine, R. *Langmuir* **2001**, *17*, 1950. (b) Jhi, S.-H.; Kwon, Y.-K.; Bradley, K.; Gabriel, J.-C. P. *Solid State Commun.* **2004**, *129*, 769. (c) Dillon, A. C.; Jones, K. M.; Bekkedahl, T. A.; Klang, C. H.; Bethune, D. S.; Heben, M. J. *Nature* **1997**, *386*, 377.

X-ray data collection and analysis including CIF files, ORTEPs, and tables of metrics for non-SQUEEZED and SQUEEZED structures. Powder X-ray diffraction patterns (simulated and experimental) for IRMOP-51, -53, and MOP-54. Magnetic susceptibility plots and TGA curves for IRMOP-51, -53, and MOP-54. This material is available free of charge via the Internet at http://pubs.acs.org.

JA042802Q